

# Off-axis parabolic mirror relay microscope for experiments with ultra-cold matter

Cite as: Rev. Sci. Instrum. **90**, 123701 (2019); <https://doi.org/10.1063/1.5123792>

Submitted: 09 August 2019 . Accepted: 29 November 2019 . Published Online: 17 December 2019

 Michal Hejduk, and  Brianna R. Heazlewood



View Online



Export Citation



CrossMark

## ARTICLES YOU MAY BE INTERESTED IN

[Submicrometric absolute positioning of flat reflective surfaces using Michelson interferometry](#)

Review of Scientific Instruments **90**, 123702 (2019); <https://doi.org/10.1063/1.5126596>

[An apparatus based on an atomic force microscope for implementing tip-controlled local breakdown](#)

Review of Scientific Instruments **90**, 123703 (2019); <https://doi.org/10.1063/1.5129665>

[Development of gamma ray spectrometer with high energy and time resolutions on EAST tokamak](#)

Review of Scientific Instruments **90**, 123510 (2019); <https://doi.org/10.1063/1.5120843>



**JANIS**  
A LAKE SHORE COMPANY

**Rising LHe costs? Janis has a solution.**  
Janis' Recirculating Cryocooler eliminates the use of Liquid Helium for "wet" cryogenic systems.

[sales@lakeshore.com](mailto:sales@lakeshore.com) [www.lakeshore.com/rgc](http://www.lakeshore.com/rgc) Click for more information.

# Off-axis parabolic mirror relay microscope for experiments with ultra-cold matter

Cite as: Rev. Sci. Instrum. 90, 123701 (2019); doi: 10.1063/1.5123792

Submitted: 9 August 2019 • Accepted: 29 November 2019 •

Published Online: 17 December 2019



Michal Hejduk<sup>a)</sup>  and Brianna R. Heazlewood<sup>b)</sup> 

## AFFILIATIONS

PTCL, Department of Chemistry, University of Oxford, South Parks Road, Oxford OX1 3QZ, United Kingdom

<sup>a)</sup>Electronic mail: [michal.hejduk@chem.ox.ac.uk](mailto:michal.hejduk@chem.ox.ac.uk)

<sup>b)</sup>URL: <http://heazlewood.chem.ox.ac.uk>

## ABSTRACT

A new optical system is introduced for the imaging of Coulomb crystals held in a cryogenic ion trap where there are space limitations preventing the placement of an objective close to the fluorescing ions. The optical system features an off-axis parabolic (OAP) mirror relay microscope that will serve to acquire images of a lattice of fluorescing ions confined within an ultra-high-vacuum vessel operating at temperatures below 10 K. We report that the OAP mirror relay setup can resolve features smaller than the separation between neighboring ions in Coulomb crystals. The setup presented here consists of two 90-degree OAP mirrors arranged into a relay from which standard microscope optics deliver the image to a camera. This design allows the first element in the imaging setup—an OAP mirror—to be located as close as possible to the ion trap, achieving high resolution without the need for a direct line-of-sight to the trap center or for a view port to be located in close proximity to the ion trap. Such an arrangement would not be possible with a standard microscope objective, which is the approach commonly adopted by the field. OAP mirrors represent a novel solution for delivering polychromatic images with micrometer-scale resolution over extended distances.

Published under license by AIP Publishing. <https://doi.org/10.1063/1.5123792>

## I. INTRODUCTION

Gas phase periodic structures of ions, known as ion Coulomb crystals (ICCs), are increasingly being adopted in a variety of scientific disciplines. In the past decade, ICCs have been employed for the study of quantum information processing, quantum simulation and computation, cosmology, chemical physics, and physical chemistry, to name a few applications.<sup>1–7</sup> Ion Coulomb crystals are produced by cooling atomic ions to subkelvin temperatures in an ion trap. After repeated cooling cycles, the ions progressively give away their momenta to photons and can eventually reach submillikelvin temperatures (0.5 mK in the case of  $\text{Ca}^+$ ).<sup>8,9</sup> In a linear radio frequency (RF) trap, as depicted in Fig. 1 (see the cut-out) and adopted in this work, the combination of oscillating and static electric potentials applied to the trap rods generates a cylindrically symmetric confining potential, whereby the ions occupy fixed positions in a crystal lattice that balances the repulsive Coulomb forces and confining trapping forces.

Laser-cooled ions within ICCs are constantly fluorescing, with neighboring ions typically separated by 10–20  $\mu\text{m}$ . As such, the lattice positions and numbers of laser-cooled ions can be directly

monitored using standard optical microscopes that project the emitted fluorescence onto appropriate camera systems [such as electron multiplying charge-coupled device (EM-CCD) cameras]. The trap itself has to be operated under ultrahigh vacuum (UHV) conditions in order for stable ICCs to be formed. Fluorescence images of the ICCs must therefore be captured through an optical view-port, with the majority (if not all) of the imaging apparatus erected outside the UHV conditions of the ion trap chamber. In experiments that require only a few access points to the trap, this view-port can take the form of a window located within a few centimeters of the trap center. A microscope objective with an appropriate working distance can then be placed close to the window to achieve optimal resolution in the images that are recorded.

It is desirable to maximize the numerical aperture (NA) in order to achieve high image resolution and to collect as much of the fluorescence signal as possible; a large NA facilitates a large photon collection angle, which is important for optimizing the signal-to-noise ratio in experiments. As can be inferred from the inset of Fig. 1, the rods of linear quadrupole ion traps limit the NA in planes perpendicular to the trap axis (i.e.,  $xy$  planes) but not in  $xz$  planes

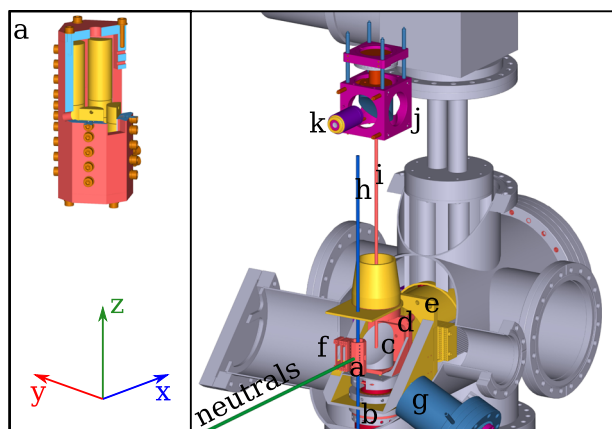


**FIG. 1.** Illustration of the new cryogenic ion trap apparatus with the key elements inside the central vacuum chamber indicated. The ion trap (a) with the interior made visible in the left panel is mounted on a vibration-isolated stage (b), and the first OAP mirror (c) is positioned close by. Two nested cryogenic shields are shown in red (d) and yellow (e), with the time-of-flight spectrometer (f) housed within the outer shield. The calcium atom beam source (g) is shown in blue. Cooling lasers (h) are directed along the central axis of the ion trap, with the resulting ICC fluorescence image (i) directed out of the vacuum chamber by the OAP mirror (c), where the second OAP mirror (j) reconstructs the image in front of the microscope objective (k). The chamber will be interfaced with a source of neutral particles traveling perpendicular to the trap axis.

including the trap axis. Therefore, using a high NA objective makes sense as it allows one to maximize the resolution and the photon collection surface.

Obtaining optical components with the appropriate characteristics is typically the most important consideration when designing an imaging setup. Often, this involves some level of compromise, both due to cost and the design of the experimental apparatus. For example, the geometry of RF ion traps physically prevents optical components from being placed within a few centimeters of the trap center. Microscope objectives with working distances on the order of 1 cm and high NAs ( $\geq 0.4$ ) can also be very expensive.

One can consider placing the first optical component—the objective—inside the UHV chamber. There are only a few commercial suppliers of appropriate low-outgassing products, and the properties of the objectives that are designed for UHV conditions are such that they do not typically offer working distances  $>1.0$  cm, limiting their usefulness for imaging ICCs in quadrupole ion traps. (Planar ion trap geometries would allow the objective to be positioned closer to the trap center, but such an arrangement comes with the risk of influencing the confining electric fields.) The outgassing rate of standard optical components can, however, be significantly reduced if the component is cryogenically cooled. This is a viable option for ion trap experiments in which cryogenic shielding is already in place to limit black-body radiation (BBR).<sup>10–13</sup> The risk associated with this approach is that very few products that are available off-the-shelf have been tested under cryogenic conditions.

In this work, we introduce a novel approach to imaging ICCs—one that achieves a comparable (if not improved) resolution to traditional imaging approaches while also being compatible with a new

cryogenic ion trap apparatus currently being constructed.<sup>7,12</sup> The need to minimize exposure to 300 K black-body radiation and to accommodate several elements close to the ion trap motivated the development of this alternative imaging setup. The new imaging apparatus exhibits all of the necessary features for an ICC imaging system, namely, a high NA, a long working distance, UHV and cryogenic compatibility, micrometer-range optical resolution, spatial ellipticalness, and cost-effectivity. All of these features are demonstrated, and all of the essential criteria for an ICC imaging setup are met. We propose that our design is highly versatile, and that it could be adopted or straightforwardly adapted for a range of other imaging applications.

## II. DESIGN

### A. Requirements for the imaging system

A new cryogenic ion trap apparatus is in the final stages of construction for the study of ion-neutral reactions in ICCs under controlled conditions. In order to study reactions between ions and a (divergent) beam of decelerated particles, it is necessary for the ion trap to be positioned as close as possible to the neutral beam source. This is combined with the need to accommodate time-of-flight mass spectrometry detection capabilities, to connect a cryocooler and to maintain line-of-sight access for the effusive Ca atom beam (in order to form the  $\text{Ca}^+$  ICCs). The design that achieves all of these requirements is shown in Fig. 1. As one can see from the schematic of Fig. 1, there is no room to incorporate a view-port window sufficiently close to the ion trap for imaging purposes.

In order to overcome this difficulty in accommodating the imaging setup, we remove the need for a straight line-of-sight to the center of the ion trap. A pair of off-axis parabolic (OAP) mirrors is arranged such that they form an optical relay, delivering an image over a long distance (see Fig. 2). This overcomes the need for a direct line-of-sight between the object and the objective and realizes the properties of a lens and a turning mirror in one optical element. One of the OAP mirrors is situated inside the UHV chamber, with the second mirror reconstructing the original image outside the vacuum chamber, where it can be freely manipulated. A similar setup was first reported by Malone *et al.*, where a pair of OAP mirrors formed part of a thermal imaging diagnostic tool for shockwave experiments.<sup>14</sup> To the best of our knowledge, such an approach has never previously been applied to the imaging of features requiring sub-10  $\mu\text{m}$  resolution. Here, we provide a robust report on the experimental performance of the system.

### B. Off-axis parabolic mirrors

Commercially available aluminum OAP mirrors with a 50.8 mm diameter, a 50.8 mm effective focal length, and a 90 degree offset angle are selected for the imaging relay. While this may sound like a large mirror surface area (given the small size of the ICCs), it is necessary to avoid geometric distortions; our Zemax simulations indicate that ICCs longer than 200  $\mu\text{m}$  in any dimension could not be imaged with a smaller OAP mirror without introducing distortions into the image. As specified by the manufacturer of the OAP mirrors (Edmund Optics), the mirror surface roughness is 50 Å

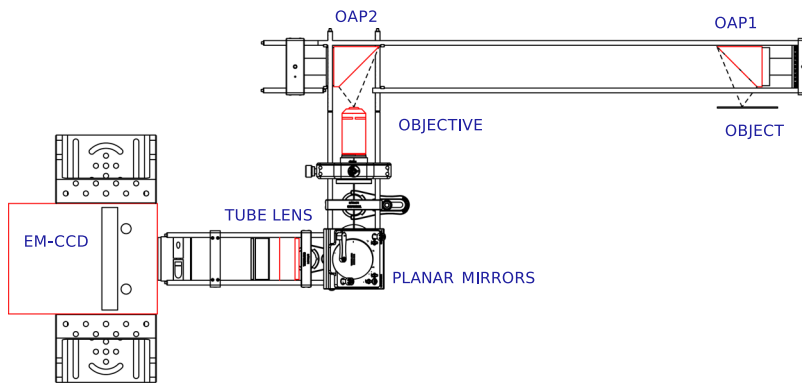


**FIG. 2.** Top view of the optical setup with the key components labeled. The object is illuminated from behind by an ultraviolet light-emitting diode (UV-LED). The dimensions and features of the optical accessories are taken from the manufacturer (Thorlabs).

and the relative focal length tolerance is 1%. The mirror surface is coated with a protective layer that has 85% reflectance at 397 nm (the wavelength of the fluorescence emitted by laser-cooled  $\text{Ca}^+$  ions of interest in this work)—slightly lower than the transmittance of fused silica (90%) lenses at the same wavelength. As the OAP mirror relay does not suffer from chromatic aberration, one could also image fluorescing species other than  $\text{Ca}^+$  ions.

As explored in detail by Malone *et al.*,<sup>14</sup> two identical OAP mirrors should be used in the mirror relay for optimal resolution. One must also consider the relative orientations of the OAP mirrors; otherwise, the image can be tilted (see Refs. 14 and 15 for an in-depth explanation of this point). Considering the properties of the OAP mirrors adopted here, the NA is approximately 0.35, which is comparable to (and, in some cases, higher than) the values reported for many off-the-shelf reflective objectives, with a significantly reduced cost. One can compare this with the  $\text{NA} = 0.28$  reflective objective that was successfully employed in the CryPTEx apparatus.<sup>10,11</sup> Despite the comparatively low NA of the objective, the CryPTEx apparatus has produced a number of exceptional results and the resolution of the imaging setup does not appear to have been a limiting factor. As such, we are confident that a NA of 0.35 will be more than sufficient for our ICC imaging requirements, as it has the power to resolve features down to the  $5\ \mu\text{m}$  level.

### III. CHARACTERIZATION

#### A. Realization of the OAP mirror relay

While our calculations indicate that the resolution achievable with an OAP mirror relay is more than adequate for our intended application, these predictions must be tested and confirmed experimentally before the system can be implemented. In particular, it is important to establish whether imperfections in the manufacturing of the mirrors impact the resolution that can be realized experimentally and how precisely the mirrors must be aligned to avoid problems with the relay of the images to the camera system. To carry out these checks and to characterize the optical properties of the system, a testing rig has been set up (see Fig. 2). A negative 1951 USAF resolution test target back-illuminated by an ultraviolet light-emitting diode (UV-LED) at a central wavelength of  $\lambda = 395\ \text{nm}$  is used as an object. The LED is located 33 cm behind the test target, with the target installed on an  $xy$  translation stage (see Fig. 3).

For resolution measurements, the mirrors are separated by a distance of 56 cm (as measured from the base of each OAP mirror). This corresponds to the minimum separation of the two OAP mirrors in the cryogenic ion trap apparatus introduced in Fig. 1. A Nikon CFI Plan Fluor microscope objective with  $\text{NA} = 0.75$  installed on an  $xyz$  translation stage serves to magnify the image reconstructed by the second OAP mirror (see Fig. 2). Light rays are then directed by a pair of planar broadband dielectric-coated elliptical mirrors to a tube lens (with an effective focal length of 200 mm) and finally on to a CCD chip. The objective, the mirrors, and the tube lens transmit 400 nm light with efficiencies of 80%, >98%, and 92% (respectively), resulting in a combined

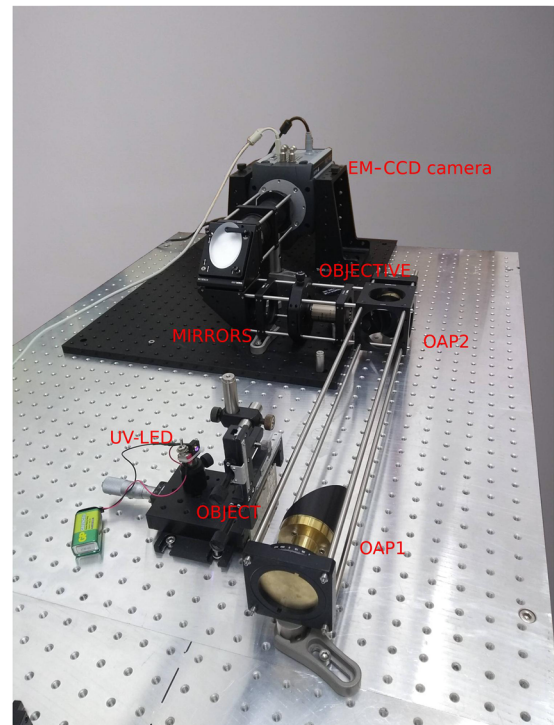


**FIG. 3.** Photograph of the testing rig employed in the characterization experiments.



transmittance of 72% for these components of the optical relay. When including the two OAP mirrors, the overall transmission from the object to the detector is 52% (for wavelengths around 400 nm). If we compare this technical solution to the imaging system of CryPTE<sub>x</sub>, i.e., an alternative composed of one reflective aluminum objective in a vacuum chamber and one tube lens, the transmission of the OAP relay-based setup is 1.5 times lower. However, the OAP mirrors also collect 1.56 times more light than the CryPTE<sub>x</sub> approach, effectively balancing the losses in transmission. It should be noted that the imaging approach utilized in the CryPTE<sub>x</sub> apparatus is not applicable to our case as we cannot maintain a straight line-of-sight. The comparison simply serves as a benchmark against which one can assess the performance of the OAP mirror-based imaging relay system.

## B. Results

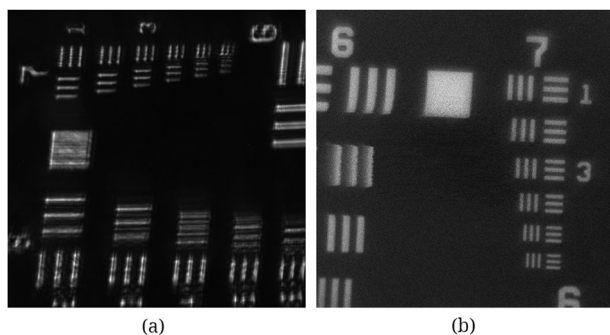
The OAP mirrors are aligned with the aid of a guide laser attached to a pinhole and situated on an *xy* translation stage. In this way, an interference pattern with a clearly localized spatial origin can be generated. The tilt of the first OAP mirror (labeled OAP1 in Fig. 2), the mutual displacement of the mirrors, and the position of the microscope objective are adjusted until the image of the interference pattern (projected on a distant wall) is minimally divergent and distorted. The quality of the alignment appears to greatly affect the image resolution: even a mutual shift of the mirrors perpendicular to their common axis by 0.2 mm can result in a 2.5-fold decrease in resolution (see below for further details).

Figure 4(a) shows the highest resolution image recorded using the OAP mirror system. It is compared to an image acquired by a microscope objective directly [Fig. 4(b)] using the same camera system. In both images, a small amount of tilting can be seen. The tilting is more evident when the OAP mirror relay is in place, which is due to the slight misalignment of the calibration target during installation. (This accidental misalignment does, however, have the benefit of illustrating the depth of field of the OAP mirror-based imaging system, which is addressed in further detail below.) The smearing of the group 6 portion of the image acquired with the OAP mirror

array [bottom right corner of Fig. 4(a)] is attributed to reflection of the UV light from the optical table. The luminosity of Fig. 4(a) is also somewhat lower as the back-illuminating LED was placed further from the target. While the OAP mirror relay does not achieve the same resolution as the traditional direct imaging approach with a microscope objective [Fig. 4(b)], it only struggles to distinguish features on the target that require a resolving power greater than 228.1 line pairs per mm (lp/mm).

In order to confirm that there is no geometric distortion of images on an experimentally relevant scale for imaging ICCs, a Ronchi ruling with 100 lp/mm at two different orientations with respect to the optical table is imaged by the OAP mirror relay. The field of view of the image is approximately  $200 \times 200 \mu\text{m}^2$ . As Fig. 5 clearly illustrates, no geometric distortion that would complicate ICC image analysis is apparent in the field of view.

As the position of an ICC in the trap depends very sensitively on the confining potentials applied to each of the rod segments, it is difficult to guarantee that the ICC will always be located in the geometric trap center. The position of the first OAP mirror with respect to the trap center will also change when the chamber is cryogenically cooled, due to thermal contraction of the mirror holder [see Fig. 1(c)]. (The thermal contraction of the OAP mirror itself is discussed in Sec. IV.) Therefore, it is necessary to ensure that there is a degree of tunability in the system; the OAP mirror relay must be able to accommodate small variations in the relative position of the first OAP mirror and the object to be imaged. The maximum resolution attainable is plotted as a function of the separation between the first OAP mirror and the target image in Fig. 6, achieved by moving the position of the resolution test target with respect to the OAP mirror using an *xy* translation stage. The full-width-at-half-maximum (FWHM, evaluated from a Lorentzian function fit to the experimental data) of the resulting curve is  $\sim 160 \mu\text{m}$ . However, if one subsequently adjusts the *xyz* stage holding the microscope objective to optimize the resolution at each of these OAP mirror-object distances, one can significantly increase the region over which high resolution can be achieved (and, thus, the volume in which ICCs can be imaged). The fully optimized OAP mirror imaging system



**FIG. 4.** Images of the same USAF resolution test target, acquired with and without the OAP mirror relay system, recorded using an EM-CCD camera. (a) The highest resolution image achieved using the OAP mirror relay microscope setup introduced in this work. (b) The image projected by a microscope objective without the OAP mirror relay.

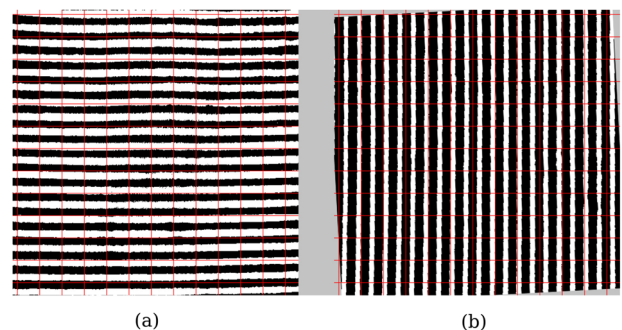


**FIG. 5.** Binarized image of a Ronchi ruling with 100 lp/mm features, recorded using the OAP mirror relay with an EM-CCD camera, with stripes oriented parallel (a) and perpendicular (b) to the bases of the OAP mirrors. A red grid has been superimposed on the images to aid the eye in evaluating the performance of the imaging relay. (a) and (b) are obtained with different resolution settings. (b) is slightly rotated to facilitate an easy comparison with the red grid. The field of view is approximately  $200 \mu\text{m} \times 200 \mu\text{m}$ .

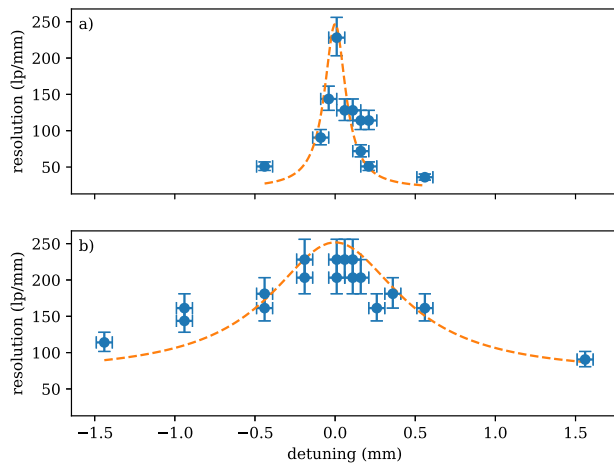


**FIG. 6.** The impact of adjusting the position of the object (detuning) with respect to the position of the first OAP mirror on the maximum achievable resolution of the OAP mirror relay system is plotted. Resolution is evaluated using a 1951 USAF resolution test target. In (a), the test target is displaced, but no other elements of the optical setup are adjusted. In (b), the position of the microscope objective is subsequently adjusted at each detuning position to optimize the resolution. The dashed lines (Lorentzian functions) serve as a guide to the eye, to aid a comparison of the two distributions.

can accommodate object displacements of  $\pm 500\ \mu\text{m}$ —a range significantly greater than the anticipated  $\sim 150\ \mu\text{m}$  shift in the mirror position due to thermal contraction of the copper holder as the temperature is lowered from 297 K to 4 K. The resolution also deteriorates if the relative orientations of the two OAP mirrors are suboptimal, consistent with previous findings,<sup>14</sup> and so the relay must be aligned with precision.

#### IV. ESTIMATION OF MIRROR BEHAVIOR UNDER CRYOGENIC CONDITIONS

As illustrated in Fig. 1 and noted above, the first OAP mirror will be fixed on a platform that will be cooled down to temperatures  $< 10\ \text{K}$ . One must therefore consider how the geometry and optical properties of the mirror will change as a result of thermal contraction. As the resolution testing cannot be performed with the OAP mirror array installed in the cryogenic chamber (due to space restrictions), we first simulate the deformation using a FEM (finite element method) approach.<sup>16</sup>

The mirror can be fixed to the holder by screws at three points, marked 1, 2, and 3 in the lower right panel of Fig. 7. There is also a hole for a centering pin (C) that can serve as an anchor. Figure 7(a) simulates the deformation that arises when the mirror is held in place only by the centering pin in hole C. In this case, the majority of the deformation to the surface area of the mirror is in the direction normal to the surface—illustrated by the arrows in Fig. 7(a), with the magnitude of the deformation represented by color. The simulated surface deformation is fairly uniform, with the exception of a small central region above the fixing point, where the deformation is anticipated to be more than an order of magnitude smaller. [Note that the magnitude of the surface deformation is expected to be near-uniform and on the order of  $2\text{--}5\ \mu\text{m}$  if the mirror is not fixed to

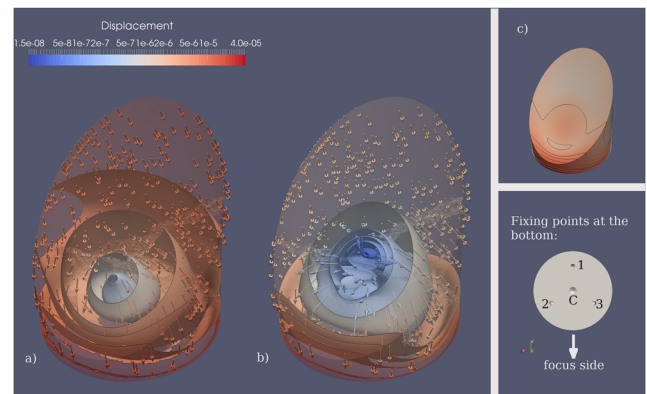


**FIG. 7.** Simulated thermal deformations of an OAP mirror at 4 K fixed to the base unit in two different ways: (a) by central rod, C, and (b) by three screws, at points 1, 2, and 3. Arrows indicate the direction of deformation, with magnitude indicated by color (with the scale bar in units of m). (c) shows the mirror surface deformation that occurs when the mirror is not fixed to the base. Isosurfaces indicate the regions with the same magnitude of deformation (see text for details).

the base, as shown in Fig. 7(c).] The central profile of the reflective surface (an intersection of the reflective surface with a plane perpendicular to the base and going through centers of holes 1 and C) deforms to a shape best fitted by an elliptic arc.

If the mirror is fixed to the base by screws in holes 1, 2, and 3, we see different behavior. As is apparent in Fig. 7(b), there is less displacement of the surface when the mirror is fixed at three points compared to the single anchor point, but the direction of the deformation is not uniform. The concavity of the reflective surface is therefore disturbed, potentially introducing larger image deformations than in the case of Fig. 7(a). In both simulations, we see that the local deviations from the original surface are on the order of several micrometers. This is large in comparison with the standard deviation indicated by the manufacturer ( $< 1/8$ th of a wave at  $632.8\ \text{nm}$ ). While we are unable to quantify the extent to which the surface deformation at cryogenic temperatures will affect the imaging properties, there are steps that can be taken to reduce the effect, for example, by fixing the mirror to the base using aluminum screws (as the mirror itself is primarily aluminum) and ensuring that the holes in the base unit (through which the mirror will be secured) have a large diameter, to allow the mirror to contract with minimal distortion.

Another issue one should consider is the spectral range over which the OAP mirror is reflective. This is of interest when considering the versatility of the OAP mirror relay. For example, if one wishes to study laser-cooled species other than  $\text{Ca}^+$ , or to be able to use the mirrors to undertake spectroscopic measurements, then the ability to transmit a range of wavelengths is desirable. Conversely, having a broad spectral region over which the OAP mirrors are reflective could direct a large portion of the 300 K black-body radiation (BBR) spectrum into the center of the ion trap. In order to reach a compromise between these conflicting requirements, the cryogenic shielding within the vacuum chamber (pictured in Fig. 1) is designed to minimize the transmission of 300 K BBR into the ion trap by using a series of nested “chimneys” to limit the solid angle. In this way,

OAP mirrors with high reflectivity over a broad spectral range can be utilized. The performance of this solution will be experimentally verified in future work.

## V. CONCLUSION

An innovative imaging system, built around two off-axis parabolic mirrors arranged into an optical relay, provides an alternative to the conventional setups employed for imaging ICCs or other samples of laser-cooled species. In particular, this work demonstrates how the requirement for a direct line-of-sight to the center of an ion trap can be overcome. This will be useful in situations where numerous additional components need to be interfaced with the ion trap; the placement of the first element in the imaging setup—an OAP mirror—close to the object negates the constraint that a view port be located immediately adjacent to the ion trap. The OAP mirror-based imaging system introduced in this work can provide the resolution necessary for imaging ICCs. An optical relay based on two OAP mirrors thus offers an uncomplicated and novel approach to delivering images over extended distances with micrometer-scale resolution.

## ACKNOWLEDGMENTS

B.R.H. acknowledges the financial support of the EPSRC (Project Nos. EP/N004647/1 and EP/N032950/1).

## REFERENCES

- <sup>1</sup>S. Willitsch, “Coulomb-crystallised molecular ions in traps: Methods, applications, prospects,” *Int. Rev. Phys. Chem.* **31**, 175–199 (2012).
- <sup>2</sup>R. Blatt and C. F. Roos, “Quantum simulations with trapped ions,” *Nat. Phys.* **8**, 277–284 (2012).
- <sup>3</sup>K. Pyka, J. Keller, H. L. Partner, R. Nigmatullin, T. Burgermeister, D. M. Meier, K. Kuhlmann, A. Retzker, M. B. Plenio, W. H. Zurek, A. del Campo, and T. E. Mehlstäubler, “Topological defect formation and spontaneous symmetry breaking in ion Coulomb crystals,” *Nat. Commun.* **4**, 2291 (2013).
- <sup>4</sup>R. C. Thompson, “Ion Coulomb crystals,” *Contemp. Phys.* **56**, 63–79 (2015).
- <sup>5</sup>B. R. Heazlewood and T. P. Softley, “Low-temperature kinetics and dynamics with Coulomb crystals,” *Annu. Rev. Phys. Chem.* **66**, 475–495 (2015).
- <sup>6</sup>A. Bylinskii, D. Gangloff, I. Counts, and V. Vuletić, “Observation of Aubry-type transition in finite atom chains via friction,” *Nat. Mater.* **15**, 717–721 (2016).
- <sup>7</sup>B. R. Heazlewood, “Cold ion chemistry within Coulomb crystals,” *Mol. Phys.* **117**, 1934–1941 (2019).
- <sup>8</sup>C. J. Foot, “The Doppler cooling limit,” in *Atomic Physics*, Oxford Master Series in Atomic, Optical, and Laser Physics Vol. 7 (Oxford University Press, Oxford, New York, 2005), pp. 188–190, oCLC: ocm57478010.
- <sup>9</sup>M. S. Safronova and U. I. Safronova, “Blackbody radiation shift, multipole polarizabilities, oscillator strengths, lifetimes, hyperfine constants, and excitation energies in  $\text{Ca}^+$ ,” *Phys. Rev. A* **83**, 012503 (2011).
- <sup>10</sup>O. O. Versolato, M. Schwarz, A. Windberger, J. Ullrich, P. O. Schmidt, M. Drewsen, and J. R. Crespo López-Urrutia, “Cold highly charged ions in a cryogenic Paul trap,” *Hyperfine Interact.* **214**, 189–194 (2013).
- <sup>11</sup>M. Schwarz, O. O. Versolato, A. Windberger, F. R. Brunner, T. Ballance, S. N. Eberle, J. Ullrich, P. O. Schmidt, A. K. Hansen, A. D. Gingell, M. Drewsen, and J. R. C. López-Urrutia, “Cryogenic linear Paul trap for cold highly charged ion experiments,” *Rev. Sci. Instrum.* **83**, 083115 (2012).
- <sup>12</sup>M. Hejduk, N. Coughlan, J. Toscano, L. S. Petralia, A. Tsikritea, J. Elworthy, H. McGhee, T. P. Softley, and B. R. Heazlewood, “(Ultra)cold ion-neutral collisions for new (astro)chemistry,” in *EPS Conference on Plasma Physics Proceedings* (EPS, Prague, 2018), Vol. 42A, p. P4-4009.
- <sup>13</sup>T. Leopold, S. A. King, P. Micke, A. Bautista-Salvador, J. C. Heip, C. Ospelkaus, J. R. Crespo López-Urrutia, and P. O. Schmidt, “A cryogenic radio-frequency ion trap for quantum logic spectroscopy of highly charged ions,” *Rev. Sci. Instrum.* **90**, 073201 (2019).
- <sup>14</sup>R. M. Malone, S. A. Becker, D. H. Dolan, R. G. Hacking, R. J. Hickman, M. I. Kaufman, G. D. Stevens, and W. D. Turley, “Design of a thermal imaging diagnostic using 90-degree off-axis parabolic mirrors,” *Proc. SPIE* **6288**, 62880Z (2006).
- <sup>15</sup>C. Brückner, G. Notni, and A. Tünnermann, “Optimal arrangement of 90° off-axis parabolic mirrors in THz setups,” *Optik* **121**, 113–119 (2010).
- <sup>16</sup>J. Ruokolainen, P. Råback, M. Malinen, T. Zwinger, and S. Sampo, CSC-Elmer (<https://www.csc.fi/web/elmer/elmer>) (2019).